A&A 635, A176 (2020)
https://doi.org/10.1051/0004-6361/201937110

Astronomy & Astrophysics

Impact of the convective mixing-length parameter α on stellar metallicity

N. Song[1,2], S. Alexeeva[1], T. Sitnova[3], L. Wang[4,5], F. Grupp[4,5], and G. Zhao[1,2]

[1] Key Laboratory of Optical Astronomy, National Astronomical Observatories, Chinese Academy of Sciences, 20A Datun Road, Chaoyang District, Beijing 100101, PR China
e-mail: nsong@nao.cas.cn; gzhao@nao.cas.cn
[2] School of Astronomy and Space Science, University of Chinese Academy of Sciences, 19A Yuquan Road, Shijingshan District, Beijing 100049, PR China
[3] Institute of Astronomy, Russian Academy of Sciences, 119017 Moscow, Russia
[4] Universitäts Sternwarte Mümchen, Scheinerstr. 1, 81679 Müchen, Germany
[5] Max-Planck-Institut für Extraterrestrische Physik, Giessenbachstr., 85748 Garching, Germany

Received 11 November 2019 / Accepted 16 February 2020

ABSTRACT

Context. Mixing-length theory is used to treat stellar convection. As a simulation in one-dimensional stellar atmospheres models, the mixing-length parameter α is calibrated from the Sun and then applied to other stars. However, there is no strong evidence to suggest that α should be the same for stars of different evolutionary stages.
Aims. We evaluate the impact of the α value on the metallicity of different types of stars and investigate the correlation between the metallicity discrepancy (Δ[Fe/H]) and stellar parameters ($T_{\rm eff}$, log g).
Methods. We selected ten well-studied field stars and one open cluster of nine members for which high-resolution and high signal-to-noise spectra are available. The model atmospheres were calculated with the code MAFAGS-OS. We derived iron abundances from Fe I and Fe II lines both under local thermodynamic equilibrium and non-LTE conditions using a spectrum synthesis method. After deriving [Fe/H] for each line, we calculated Δ[Fe/H] with two different α values, fixed solar-calibrated α, and α obtained for each star individually. Finally, we investigated the correlation between Δ[Fe/H] caused by revised α with stellar parameters.
Results. For FGK dwarf stars, the Δ[Fe/H] caused by the α correction is less than 0.02 dex, while for turn-off and giant stars, the Δ[Fe/H] values are no more than 0.03 dex, which are lower than typical uncertainties in metallicity. For main-sequence stars, Δ[Fe/H] versus $T_{\rm eff}$ and Δ[Fe/H] versus log g are well fit by linear relations.

Key words. stars: atmospheres – stars: abundances – stars: fundamental parameters – convection – line: profiles

1. Introduction

Convection plays a crucial role in the modeling of stellar atmospheres. With a one-dimensional (1D) stellar model, Böhm-Vitense (1958) used mixing-length theory (MLT) to describe convective energy transport. Classical MLT treats convection as a single characteristic length that is proportional to the local pressure scale height $l = \alpha H_{\rm p}$. In this case, the mixing-length parameter α is a free parameter that represents the efficiency of convection and $H_{\rm p}$ is the pressure scale height. Canuto & Mazzitelli (1991, 1992) described a new formalism, which includes the full spectrum of turbulent eddies instead of only a single eddy size.

Ludwig et al. (1999) calibrated α for solar-type stars with 2D hydrodynamic models. Because there is not enough calibration stars to determine the α value through precise stellar parameters except the Sun, most stellar models generally treat convection in stellar envelopes with MLT and the universal solar-calibrated α value. That value has been adopted as constant along the stellar evolutionary track in most cases, even though we know that the properties of convection depend on stellar parameters, such as effective temperature, surface gravity, and metallicity.

With the development and refinement of stellar models and the improvement of computing power, recently, several studies focused on the calibration mixing-length parameter α by matching averages of the 3D radiative hydrodynamic simulations to 1D stellar envelope models (Trampedach et al. 2014; Magic et al. 2015). Through analysis with 3D simulations, some potential relations between α and other stellar atmosphere parameters were revealed. Magic et al. (2015) (hereafter M15) calibrated mixing-length parameters for a grid of various stellar parameters that could be used to replace a constant value for stars in different evolutionary phases. Their result suggested that the solar α value is not always applicable for different types of stars. These authors performed individual functional fits of the mixing-length parameters with $T_{\rm eff}$ and log g for different metallicities.

In addition to the theoretical simulation work we mentioned above, other investigations focused on their analysis of α by comparing the models with observed astroseismological data. Bonaca et al. (2012) studied the correlation between α and stellar properties with astroseismic data from NASA's *Kepler* mission for dwarfs and subgiants. These authors found a significant correlation between metallicity and α. Viani et al. (2018) expanded upon the sample of stars used in Bonaca et al. (2012). Viani et al. (2018) found that the value of α could be approximated by a linear model in the form of $\alpha/\alpha_{\odot} = 5.426 - 0.101\log(g) - 1.071\log(T_{\rm eff}) + 0.437([{\rm Fe/H}])$. They suggested that the uncertainties in α need to be added to the error budget of results that use single-valued α models whenever possible. On the other hand, Valle et al. (2019) analyzed the theoretical foundation and

statistical reliability of the mixing-length calibration by means of standard ($T_{\rm eff}$, [Fe/H]) and global asteroseismic observables (the large frequency separation $\Delta\nu$ and the frequency of maximum oscillation power $\nu_{\rm max}$) of field stars. These authors pointed out that any claim about the possible dependence of the mixing length on the metallicity for field stars should be considered cautiously and critically.

As the closest binary system to Earth, the mixing length of α Centauri A and B have been studied in detail (Guenther & Demarque 2000; Miglio & Montalbán 2005; Joyce & Chaboyer 2018a). Other star samples were also selected to derive more accurate α values and detailed analyses. Chun et al. (2018) calibrated α by comparing the most recent observations of red supergiants (RSGs) with stellar evolution models at various metallicities. It was shown that α increases as metallicity increases for RSGs. Joyce & Chaboyer (2018b) focused on metal-poor stars both in the field and in globular cluster M92 at different evolutionary phases. These authors found that subsolar mixing-lengths were necessary to achieve agreement with observations for low metallicity ([Fe/H] ≈ -2.3) stars.

For the calculation of stellar model atmospheres, the mixing-length parameter should be considered, where α is fixed to solar-calibrated value in most cases. The solar-calibrated value is usually adopted in the case of relatively large samples. The most popular model codes, ATLAS (Kurucz 1993; Castelli & Kurucz 2004) and MARCS (Gustafsson et al. 2008), only provide fixed α values to treat convection for the atmospheric grids. The fixed α is just a reasonable simplification to deal with convection under MLT, since it is difficult and time consuming to calculate α individually for each star in a large sample. There is no theoretical justification that the same value of α should apply for different types of stars. In this paper, we aim to estimate the impact of the convective mixing-length parameter α on metallicity and determine how metallicity changes when we adopt the updated calibrated α value compared to the solar-calibrated value for different star types.

The paper is organized as follows. Section 2 introduces the star samples and spectral sources. Our analytical method is described in detail in Sect. 3. Section 4 includes the results and discussion. We compare our results from 1D simulations with previous studies that use 3D convective simulations. Section 5 gives our conclusions and suggestions for future work.

2. Star samples and observations

We selected two sample of stars for our analyses. The first is the well-studied field star sample from Wu et al. (2015) (hereafter W15). The W15 sample comprises ten stars in a relatively large parameter space, with effective temperatures ($T_{\rm eff}$) from 4600 to 6600 K and metallicities ([Fe/H]) from −2.6 to +0.5. The field star sample has one giant star and two subgiants. All the stars have been observed by Fiber Optics Cassegrain Echelle Spectrograph (FOCES; Pfeiffer et al. 1998) on the 2.2 m telescope at Calar Alto Observatory. They selected a representative field star sample, calculated high precision atmospheric parameters, and recalibrated the α value with convincing analyses. Our second sample consists of member stars from the open cluster Melotte 111, which were selected by Grupp (2004a). Compared to the field star sample, the cluster stars represent a relative homogeneous sample with similar iron metallicity at different stages of evolution. The Melotte 111 star cluster (also called the Coma Berenices cluster) is the second closest open cluster to us (85.86 pc; Gaia Collaboration 2018). It is a sparse cluster and covers a relatively large area on the sky. Silaj & Landstreet (2014) derived the precise age of 560 ± 90 Myr. Trumpler (1938) gave a labeled catalog of stars that are brighter than 10.5 mag in this area and identified 37 members. Subsequent work revealed a small number of additional members (Bounatiro 1993; Casewell et al. 2006; Mermilliod et al. 2008). This open cluster provides excellent member stars for starting our research, mainly because of their coeval nature and known distances, ages, and metallicities. Member stars of this open cluster are at different evolutionary stages, which cover 4500 K < $T_{\rm eff}$ < 8500 K, including one giant star Tr 39. We hope to use these two different star samples to derive the potential correlation between the metallicity discrepancy caused by α corrections and other stellar parameters, such as effective temperature and surface gravity.

The solar spectrum we used was taken from the Kitt Peak Solar Flux Atlas (Kurucz et al. 1984). All the spectra taken from FOCES have high signal-to-noise ratios ($S/N(\rm H_\alpha) > 200$) and high resolving powers ($R = 60\,000$ for Vmag < 8.0 and $R = 42\,000$ for Vmag > 8.0), which ensures that the following line-analysis results in detailed and accurate profiles. Data reduction was performed using the FOCES EDRS software package (see Pfeiffer et al. 1998). Normalization was performed manually.

3. Method

3.1. Iron line list

In order to analyze the iron metallicity with an appropriate line list, we adopted the iron line list from Mashonkina et al. (2011) (hereafter M11). Their line list includes 56 lines of Fe I and 18 lines of Fe II. This line list was extracted from the Kurucz (1993) compilation and VALD database (Kupka et al. 1999).

We used line list from M11 for the following reasons: first, M11 had done a detailed analysis with these lines for the Sun; second, in our field star sample we have three stars in common with M11 (HD 122563, HD 10700, and Proycon); third, HD 122563, as a very metal-poor star, was analyzed by M11, which means the line list could be applied to a widely metallicity range of stars; and fourth, the metallicity of the members from cluster Melotte 111 is close to solar metallicity. For each solar iron line the authors of M11 provided the abundances under both local thermodynamic equilibrium (LTE) and non-LTE (NLTE). We can test our results of metallicity determination by comparing our result with M11.

3.2. Stellar atmosphere parameters and recalibrated α values

We postulated that our samples consist of the stars with accurate stellar atmospheric parameters. Two stellar atmospheric models were calculated for each star. These two stellar models contained the same parameters ($T_{\rm eff}$, log g), except for two different α values. One was fixed to 0.82 with the convection theory of Canuto & Mazzitelli (1991, 1992), which was able to fit both the Sun at its present evolutionary stage and its Balmer line spectrum (Bernkopf 1998). Another one was calculated based on the new calculation for each star individually. For the field star sample, we adopted the new calibrated α from W15 directly. The revised α for open cluster stars were interpolated based on M15. Model atmospheres were calculated through the MAFAGS-OS code (Grupp 2004b,c).

The Sun is the best-known star with accurate physical parameters. We used the same solar parameters, $T_{\rm eff} = 5777$ K, log g = 4.44, [Fe/H] = 0.0 and $\xi = 0.90$ km s^{-1}, as in M11. With the same

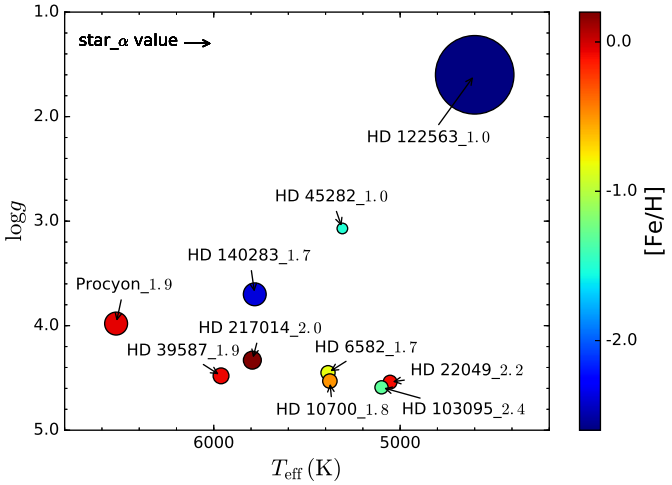

Fig. 1. Field stars on the HR diagram. The star name and recalibrated α value are labeled. The size of the circle represent the stellar diameter, which is provided by W15 through interferometric measurements.

Table 1. Basic parameters of member stars in Melotte 111.

Name	Vmag	$T_{\rm eff}$ (K)	$\log g$	$v \sin i$ (km s^{-1})
Tr 387 (*)	5.75	8430 ± 125	3.90 ± 0.10	57.5 ± 3
Tr 183	6.28	8325 ± 125	3.87 ± 0.10	9.8 ± 1
Tr 36 (*)	8.09	6600 ± 75	4.29 ± 0.07	36.0 ± 1
Tr 118	8.34	6460 ± 60	4.30 ± 0.06	16.2 ± 1
Tr 114	8.57	6370 ± 50	4.34 ± 0.06	15.0 ± 1
Tr 53	8.69	6170 ± 50	4.39 ± 0.05	5.5 ± 1
Tr 65	9.02	5980 ± 50	4.44 ± 0.05	8.5 ± 1
Tr 85	9.31	5890 ± 50	4.45 ± 0.05	4.5 ± 1
Tr 12	9.54	5790 ± 75	4.49 ± 0.07	4.5 ± 1
Tr 399 (*)	4.93	5670 ± 75	3.02 ± 0.12	64.0 ± 3
Tr A13	10.51	5360 ± 100	4.53 ± 0.10	2.8 ± 1
Tr 39	4.95	4930 ± 100	2.76 ± 0.12	1.5 ± 1

Notes. (*)Eliminated from the open cluster sample in the following spectral synthesis analysis because of high rotational velocity.

atmosphere model calculated by MAFAGS-OS and the same line list we mentioned above, we could verify our method and the accuracy of the abundance determinations. The solar composition adopted in the MAFAGS-OS code was taken from Lodders et al. (2009).

For the field star sample, we used the reliable stellar atmosphere parameters directly from W15. The W15 authors used interferometric parameters to determine effective temperature and calculated the $\log g$ from HIPPARCOS parallaxes. Metallicity ([Fe/H]) and microturbulence velocity (ξ) were determined by a spectroscopic method. They used the method of Fuhrmann et al. (1993) to calculate the new α value from Balmer line fitting. The recalibrated α and $T_{\rm eff}$ were determined together through the χ^2 minimization procedure. All the parameters of this sample could be found in Table 1 of W15.

We plotted ten field stars on the Hertzsprung-Russell (HR) diagram (Fig. 1) labeled with revised convective mixing-length parameters. The different colors of the circles indicate the initial metallicity for each star derived by W15. The metallicities of three evolved stars in this sample have a relatively lower values compared to the dwarf stars. Based on the determination by W15, α is consistent with a value of about 2.0 for the dwarf stars. That confirms the behavior and numerical values predicted by M15. For the three metal-poor evolved stars, the α values are relatively lower than for the dwarf stars, which is in agreement with Joyce & Chaboyer (2018b). While on the other hand, M15 suggested higher values from their 3D simulation results. In order to check the potential relationship between Δ[Fe/H] with revised α and other stellar parameters, we adopted all the stellar parameters and α values from W15 to maintain consistency.

For the open cluster sample, the initial stellar atmosphere parameters were taken from Grupp (2004a), where $\alpha = 0.82$ was adopted. We list these parameters in Table 1. The effective temperatures were rectified with new α values calculated with the method from M15.

We obtained new $T_{\rm eff}$ from fitting the wings of the Balmer lines, H_α, H_β, and H_γ (H_γ was possible only for the hottest cluster stars in our sample, Tr 387 and Tr 183). Theoretical hydrogen line profiles calculated with NLTE populations were taken into account. For stars with $T_{\rm eff} \leq 6600$ K (except for Tr 53), we found better fits, when the new α was adopted. For Tr 53, we also adopted the new $T_{\rm eff}$ even though the newly calculated $T_{\rm eff}$ is higher by 60 K. In the case of the hotter stars, Tr 387 and Tr 183, where hydrogen line profiles are more sensitive to the convection parameter, the initial $T_{\rm eff}$ were reduced by 100 K. More details about the NLTE calculations of hydrogen line profiles and the fitting of Balmer line wings are provided in W15.

After deriving the updated $T_{\rm eff}$, we reproduced the atmosphere model and recalculated $\log g$. By fitting the strong line wings of the Mg Ib triplet as Fuhrmann et al. (1997) mentioned, we determined the surface gravity through this spectroscopic method. For the cool stars in the sample, we also used *Gaia* DR2 parallaxes (Gaia Collaboration 2018) to calculate the $\log g$ of several stars with the method described in Nissen et al. (1997) for comparison. After this comparison, we finally used $\log g$ as determined by the spectrum fitting method.

Three stars (Tr 387, Tr 36, and Tr 399) in this sample have a high rotational velocity ($v \sin i$). In the following spectral synthesis analysis, we note that the rotational broadening makes it difficult to get a good fit profile and derive accurate abundance. We attempted to measure better fits for these three stars using a different model because it is not conducive to compare the abundance differences between different stellar atmosphere models. Because of the bad fits, we eliminated these three stars from the following abundance analysis.

We plotted the members of the open cluster in an HR diagram (Fig. 2). The PARSEC (PAdova and TRieste Stellar Evolution Code) isochrones (Marigo et al. 2017) are also plotted. We determined the best-fitting isochrone (708 Mry with $Z = 0.02$) to the data by plotting a grid of different isochrones with our sample stars. The largest number of stars are closest to this theoretical isochrone. This gives credence to the reliability of the derived stellar parameters.

Magic et al. (2015) performed functional fits of the mixing-length parameter $f(x, y)$ with $T_{\rm eff}$ and $\log g$ for different metallicities individually. They use 3D theoretical model atmospheres to predict the standard MLT α by Böhm-Vitense (1958) formulation with 1D model. They transformed the stellar parameters with $x = (T_{\rm eff} - 5777)/1000$ and $y = \log g - 4.44$. The fitting function is

$$f(x, y) = a_0 + (a_1 + (a_3 + a_5 x + a_6 y)\, x + a_4 y)\, x + a_2 y. \quad (1)$$

The coefficients a_i are listed in their Table B.1 for a grid of different metallicities. The a_i were calculated by interpolation for

Table 2. Stellar parameters and iron abundances under different models of the field star sample.

Object	$T_{\rm eff}$ (K)	log g	α [a]	Ion	N [b]	[Fe/H] with error, LTE			[Fe/H] with error, NLTE		
						Old	New	Δ[Fe/H] [c]	Old	New	Δ[Fe/H] [c]
HD 6582	5370	4.51	1.7	Fe I	23	-0.782 ± 0.057	-0.790 ± 0.054	-0.008	-0.791 ± 0.061	-0.800 ± 0.061	-0.009
				Fe II	7	-0.844 ± 0.033	-0.866 ± 0.040	-0.022	-0.846 ± 0.033	-0.866 ± 0.040	-0.020
HD 10700	5330	4.53	1.8	Fe I	22	-0.486 ± 0.045	-0.495 ± 0.045	-0.009	-0.500 ± 0.050	-0.508 ± 0.053	-0.008
				Fe II	8	-0.542 ± 0.038	-0.554 ± 0.041	-0.012	-0.541 ± 0.040	-0.554 ± 0.041	-0.013
HD 22049	5045	4.61	2.2	Fe I	22	-0.051 ± 0.036	-0.052 ± 0.036	-0.001	-0.070 ± 0.055	-0.074 ± 0.056	-0.004
				Fe II	9	-0.088 ± 0.033	-0.080 ± 0.031	0.008	-0.088 ± 0.033	-0.080 ± 0.031	0.008
HD 39587	5960	4.48	1.9	Fe I	16	0.086 ± 0.057	0.083 ± 0.060	-0.003	0.072 ± 0.071	0.068 ± 0.070	-0.004
				Fe II	8	0.148 ± 0.091	0.146 ± 0.086	-0.002	0.148 ± 0.091	0.145 ± 0.084	-0.003
HD 103095	5100	4.59	2.4	Fe I	21	-1.270 ± 0.039	-1.274 ± 0.044	-0.004	-1.288 ± 0.042	-1.292 ± 0.050	-0.004
				Fe II	8	-1.350 ± 0.048	-1.332 ± 0.049	0.018	-1.349 ± 0.049	-1.332 ± 0.049	0.017
HD 122563	4600	1.60	1.0	Fe I	16	-2.770 ± 0.078	-2.791 ± 0.076	-0.021	-2.580 ± 0.094	-2.601 ± 0.094	-0.021
				Fe II	10	-2.522 ± 0.043	-2.544 ± 0.046	-0.022	-2.522 ± 0.043	-2.544 ± 0.046	-0.022
HD 217014	5780	4.28	2.0	Fe I	24	0.269 ± 0.042	0.270 ± 0.042	0.001	0.251 ± 0.053	0.251 ± 0.054	0.000
				Fe II	11	0.300 ± 0.071	0.302 ± 0.072	0.002	0.300 ± 0.071	0.302 ± 0.074	0.002
HD 45282	5310	3.07	1.0	Fe I	26	-1.412 ± 0.043	-1.433 ± 0.042	-0.021	-1.233 ± 0.085	-1.253 ± 0.081	-0.020
				Fe II	9	-1.498 ± 0.029	-1.517 ± 0.026	-0.019	-1.498 ± 0.029	-1.517 ± 0.026	-0.019
HD 140283	5780	3.70	1.7	Fe I	12	-2.423 ± 0.082	-2.454 ± 0.072	-0.031	-2.363 ± 0.081	-2.397 ± 0.076	-0.034
				Fe II	2	-2.375 ± 0.078	-2.405 ± 0.078	-0.030	-2.375 ± 0.078	-2.405 ± 0.078	-0.030
HD 61421 (Proycon)	6524	3.98	1.9	Fe I	18	-0.073 ± 0.072	-0.073 ± 0.066	0.000	-0.049 ± 0.062	-0.051 ± 0.057	-0.002
				Fe II	9	-0.038 ± 0.034	-0.044 ± 0.037	-0.006	-0.038 ± 0.034	-0.044 ± 0.037	-0.006

Notes. [a]New α value derived from W15. [b]Number of iron lines used to calculate the abundances. [c]Abundance derived from new α value model minus abundance derived from old (fixed) α value.

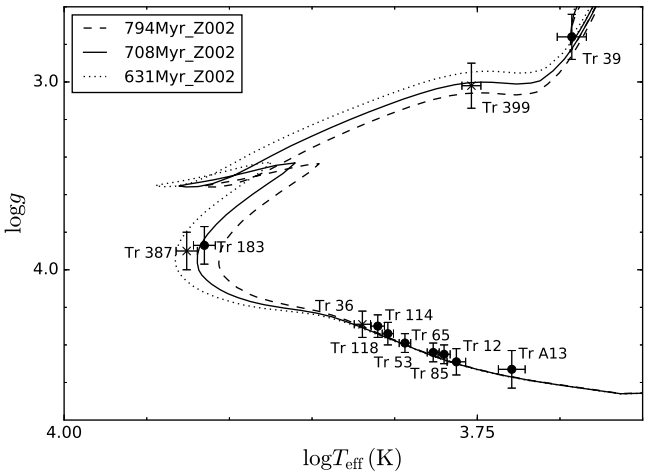

Fig. 2. Position of the member stars from the open cluster Mel 111 in the log $T_{\rm eff}$–log g plane. The nine stars that were finally adopted for analysis are labeled with black points. The three stars with rotation speeds too high to determine the abundances are labeled with an x. The PARCSEC isochrones of 794, 708, and 631 Myr are overplotted.

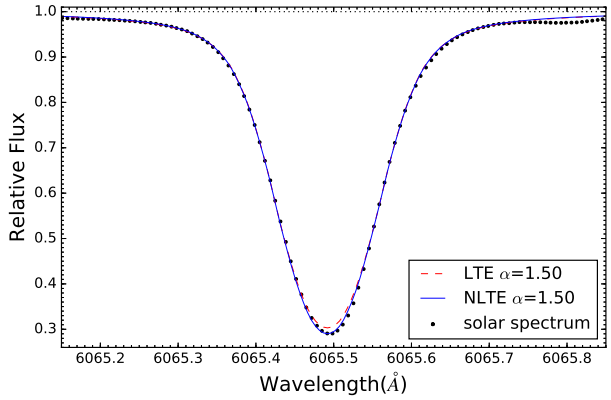

Fig. 3. Best LTE and NLTE fits of the solar Fe I λ6065Å line calculated by SIU with $\alpha = 1.5$. The abundances of these two fitting lines were log $\varepsilon_{\rm LTE} = 7.53$ (LTE) and log $\varepsilon_{\rm NLTE} = 7.55$ (NLTE). The LTE and NLTE profiles were convolved with a macroturbulence broadening of 3.0 and 3.2 km s^{-1}, respectively.

each star. For our open cluster members, we derived the α values from the functional fits. The updated temperatures and new α for stars in the open cluster are listed in Table 3.

3.3. Iron abundances

The iron abundances derived with different models and line formation scenarios are presented in Table 2. For each star and the Sun we derived iron abundances from all possible detectable Fe I and Fe II lines both under LTE and NLTE conditions using the spectrum synthesis method through the Spectrum Investigation Utility (SIU; Reetz 1999). The absolute iron abundance from each solar iron line was adopted to carry out a line-by-line differential analysis. We derived metallicities, [Fe/H]$_{\rm LTE}$ and [Fe/H]$_{\rm NLTE}$, with both α values, namely, 0.82 (solar-calibrated) and the new α calibrated for each star individually. Figure 3 presents an example of the best LTE and NLTE fit to the solar Fe I λ6065Å line calculated by SIU with $\alpha = 1.5$.

The broadening mechanism caused by instrumental, rotation, and macroturbulence have been considered during the

analysis. For the analysis of the solar spectrum, each line profile is convolved with a fixed rotational broadening of 1.8 km s^{-1} and broadening by macroturbulence with a radial-tangential profile. The macroturbulence we adopted for the sun varied between 2.6 and 3.3 km s^{-1} for different lines of neutral iron and between 3.4 and 3.8 km s^{-1} for Fe II lines. When we analyzed the FOCES spectra of our sample stars, instrumental broadening is convolved with a Gaussian profile. We adopted 4.6 km s^{-1} for the spectra with resolution 40 000 and 3.2 km s^{-1} for the spectra with resolution 65 000. We used one Gaussian profile as rotational and macroturbulence broadening together by convolving it with the spectral line. We also took into account NLTE effects for iron lines for these stars.

During the spectral synthesis calculation, we eliminated bad lines, for example, heavily blended lines that are hardly separate and lines that are too weak. We also measured the equivalent width (W_λ) of each line and excluded very strong lines whose W_λ were greater than 150 mÅ. Finally, the most reliable lines were selected to determine the abundances. The number of lines used to calculate the abundance for each star is shown in Table 2. The statistical abundance error is the dispersion in the single line measurements, $\sigma = \sqrt{\Sigma(x - x_i)^2/(N-1)}$, where N is the total number of lines used to calculate the final abundance (we excluded the 3σ outliers); x is their mean abundance; and x_i is the abundance of each individual line.

3.4. NLTE correction

This section presents our NLTE investigation for Fe I and Fe II based on Fe I-II model atom developed by M11 and updated with accurate data for inelastic collisions with hydrogen atoms from Yakovleva et al. (2018, 2019) for Fe I and Fe II, respectively. An impact of the update on NLTE results for Fe I-II has been presented by Mashonkina et al. (2019). To solve the coupled radiative transfer and statistical equilibrium equations, we employed a revised version of the DETAIL code (Butler & Giddings 1985) based on the accelerated lambda iteration (ALI) method described in Rybicki & Hummer (1991, 1992). The revision was described in detail in M11.

3.5. Metallicity discrepancy Δ [Fe/H]

We define the discrepancy in metallicity (Δ[Fe/H]) as which $\Delta[\mathrm{Fe/H}] = [\mathrm{Fe/H}]_{\alpha_{\rm new}} - [\mathrm{Fe/H}]_{\alpha_{\odot=0.82}}$. For example, $\Delta[\mathrm{Fe/H}]^{\rm Fe\,I}_{\rm NLTE}$ means the deviation in metallicity, determined from Fe I lines with NLTE approach. Finally, we investigated the correlation between Δ[Fe/H] caused by revised α with stellar parameters.

4. Results and discussion

4.1. Solar iron lines

Solar iron abundances obtained from Fe I and Fe II lines are consistent with those obtained by M11 (Fig. 4). There is a slight overall offset between our results and the M11 results for both the LTE and NLTE Fe I and Fe II line cases. Our average solar metallicity is about 0.03 dex lower than that of M11. We attribute this offset to systematic deviation. Since we adopt line-by-line differential analysis based on the solar iron abundances determined in this work, the overall offset does not affect the abundance discrepancy analysis and the final result. The 0.03 dex metallicity offset between the solar iron line reflects only the zero point offset or the systematic differences between our analysis and that of M11. The abundance discrepancies of each star with two different α values are not influenced by the abundance offset of solar iron lines in Fig. 4 when we apply line-by-line differential analysis.

4.2. Field star sample from W15

The obtained metallicities are presented in Table 2. The NLTE corrections, $[\mathrm{Fe/H}]_{\rm NLTE} - [\mathrm{Fe/H}]_{\rm LTE}$, could be identified easily in most stars in our sample, especially for metal-poor stars. We calculated more than 12 Fe I lines and a maximum of 11 FeII lines for each of the ten sample stars to derive the metallicity. In two low metal-poor stars (HD 122563, HD 140283), the values $[\mathrm{Fe/H}]_{\rm NLTE} - [\mathrm{Fe/H}]_{\rm LTE}$ obtained from Fe I lines are larger than 0.1 dex. For the Fe II lines, the values $[\mathrm{Fe/H}]_{\rm NLTE} - [\mathrm{Fe/H}]_{\rm LTE}$ are smaller than 0.01 dex in absolute values for all stars, independent of the different α models. Our NLTE corrections are in agreement with Asplund (2005) and M11, who presented that NLTE effects are not relevant for Fe II lines and mostly relevant for Fe I lines in low metallicity stars ([Fe/H] ≤ -1.0).

The metallicity discrepancy Δ[Fe/H] values are presented on the HR diagram (Fig. 5) in order to trace the potential trend along $T_{\rm eff}$ and $\log g$. We provided both the LTE and NLTE results for Fe I and Fe II lines. Regarding the Fe I lines, almost all stars except for HD 217014 have overestimated abundances with the old fixed solar-calibrated α (0.82) compared to the recalibrated α. For the seven main-sequence stars in our sample, the values of $|\Delta[\mathrm{Fe/H}]|$ are less than 0.01 dex in both LTE and NLTE cases. However, the values of $|\Delta[\mathrm{Fe/H}]|$ of the three evolved stars is larger than 0.02 dex. For the Fe II lines, Δ[Fe/H] for all different kinds of stars do not exceed 0.03 dex in absolute value.

We find no correlation between Δ[Fe/H] derived from both groups of Fe I and Fe II lines and the two stellar parameters, $T_{\rm eff}$ and $\log g$, in this field star sample. We find a slight correlation between Δ[Fe/H] and [Fe/H] (Fig. 6). Except the outliers (HD 103095 and HD 217014 of Fe I), the lower [Fe/H] star has an even lower Δ[Fe/H] value in most cases. Δ[Fe/H] and [Fe/H] can be fitted with a liner function. This result can indicate the dependence of α with metallicity which is in line with results from Bonaca et al. (2012) and Viani et al. (2018).

We use $\Delta\alpha = \alpha_{\rm revised} - \alpha_{\odot}(0.82)$ to indicate the α changes and we adopt the revised mixing-length value from W15 for the two giant stars (HD 122563 and HD 45282). We use $\alpha_{\rm giants} = 1$ for both, which means $\Delta\alpha$ is only 0.18 for these stars. For the dwarf stars, the α values are all greater than 1.7 ($1.7 \leq \alpha_{\rm dwarfs} \leq 2.4$), which means $\Delta\alpha$ for dwarf stars is larger than 0.88. Therefore, in the field star sample, the giant stars with a lower $\Delta\alpha$ get a relatively higher Δ[Fe/H] compared to the dwarf stars. We can assume that the iron metallicity of giant stars is more sensitive to $\alpha_{\rm revise}$ than that of dwarfs based on this result.

4.3. Stars in open cluster Melotte 111

The metallicities and Δ[Fe/H] values derived from Fe I and Fe II lines under the old and new α values with LTE and NLTE are listed in Table 3. Because Melotte 111 has similar metallicity to the Sun, the majority of the member stars provide more reliable iron lines for line profile fitting compared to the above field star sample. With over 30 Fe I and 10 Fe II lines, we achieve more reliable abundances for the cluster members, which make Δ[Fe/H] between the new and old α models more persuasive. Since all stars have similar metallicity ([Fe/H] $\approx$ 0.00), we can study the potential correlation between Δ[Fe/H] caused by

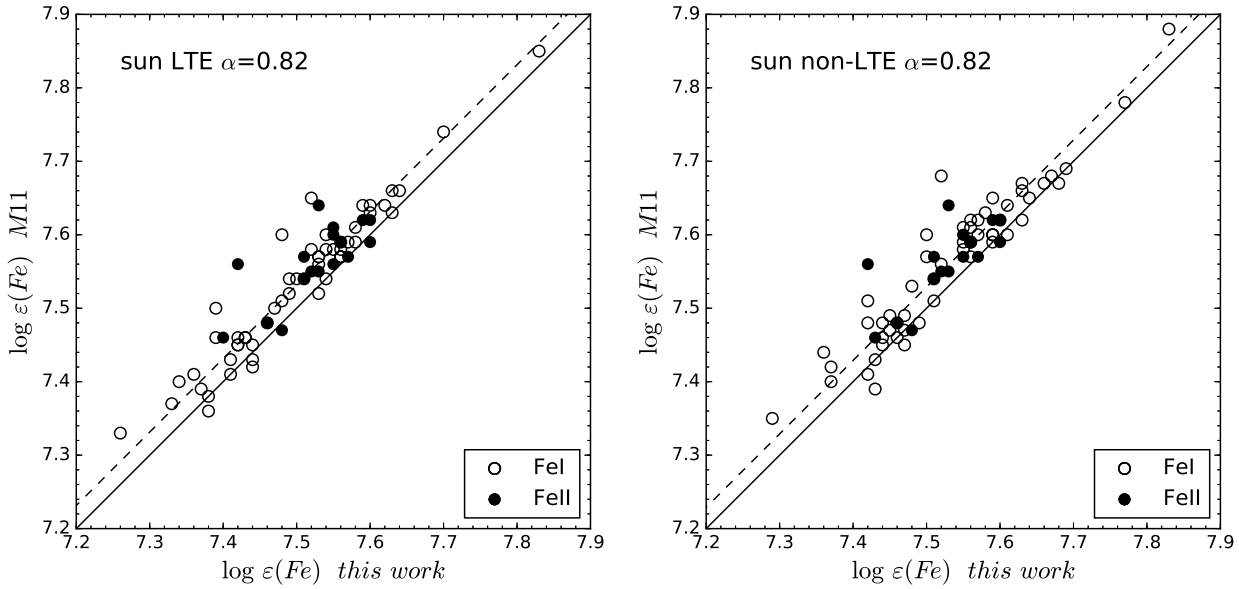

Fig. 4. Comparison between our iron abundances and the results derived from M11 under LTE (*left panel*) and NLTE (*right panel*) cases. The abundances obtained from Fe I lines are plotted with open circles and Fe II are plotted with filled circles. The dash line shows the Fe I offset from the metallicity 1:1 solid line, which is 0.031 dex under LTE and 0.029 dex under NLTE.

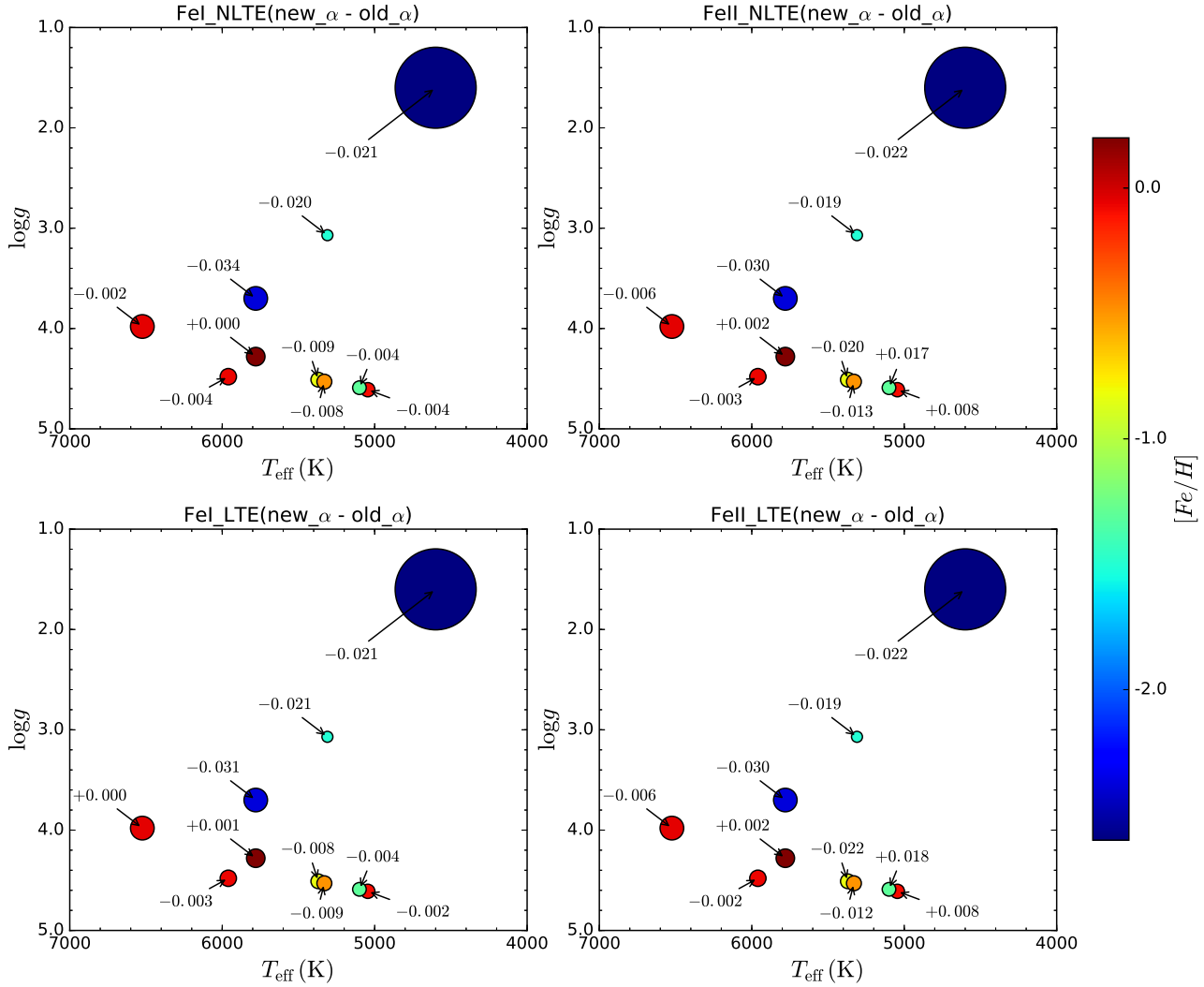

Fig. 5. Discrepancy in [Fe/H] between old and revised α for the field star sample on the HR diagram. The Δ[Fe/H] values are labeled beside each star's circle marker with an arrow.

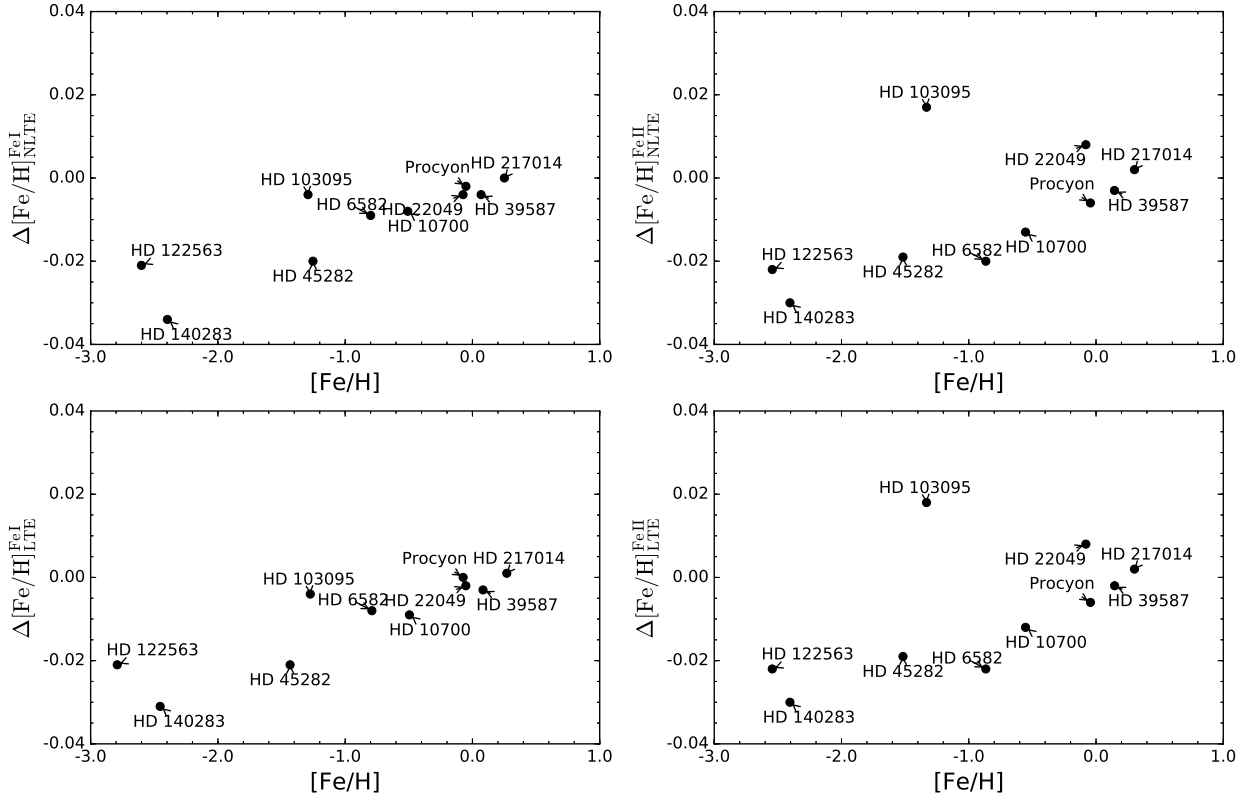

Fig. 6. Discrepancy in [Fe/H] between old and revised α for the field star sample as function of [Fe/H].

Table 3. Stellar parameters and iron abundances with different models of the open cluster sample.

Object	$T_{\rm eff}$ (K)	log g	$\alpha^{(a)}$	Ion	$N^{(b)}$	[Fe/H] with error, LTE			[Fe/H] with error, NLTE		
						Old	New	Δ[Fe/H]$^{(c)}$	Old	New	Δ[Fe/H]$^{(c)}$
Tr 183	8225	3.87	1.50	Fe I	13	-0.004 ± 0.071	-0.030 ± 0.067	-0.026	0.007 ± 0.067	-0.018 ± 0.062	-0.025
				Fe II	5	0.064 ± 0.079	0.042 ± 0.076	-0.022	0.064 ± 0.079	0.042 ± 0.076	-0.022
Tr 118	6460	4.30	1.97	Fe I	19	-0.010 ± 0.069	-0.026 ± 0.065	-0.016	-0.002 ± 0.069	-0.016 ± 0.064	-0.014
				Fe II	6	0.040 ± 0.057	0.020 ± 0.075	-0.020	0.040 ± 0.057	0.020 ± 0.075	-0.020
Tr 114	6370	4.34	2.00	Fe I	16	-0.046 ± 0.052	-0.059 ± 0.048	-0.013	-0.039 ± 0.052	-0.052 ± 0.050	-0.013
				Fe II	7	-0.026 ± 0.048	-0.041 ± 0.053	-0.015	-0.026 ± 0.048	-0.041 ± 0.053	-0.015
Tr 53	6220	4.39	2.04	Fe I	37	-0.032 ± 0.056	-0.041 ± 0.054	-0.009	-0.024 ± 0.056	-0.035 ± 0.055	-0.011
				Fe II	12	-0.095 ± 0.032	-0.106 ± 0.033	-0.011	-0.096 ± 0.033	-0.106 ± 0.033	-0.010
Tr 65	5980	4.44	2.06	Fe I	35	-0.051 ± 0.068	-0.054 ± 0.066	-0.003	-0.043 ± 0.066	-0.046 ± 0.064	-0.003
				Fe II	13	-0.018 ± 0.025	-0.024 ± 0.035	-0.006	-0.018 ± 0.025	-0.024 ± 0.035	-0.006
Tr 85	5890	4.45	2.04	Fe I	35	-0.038 ± 0.062	-0.040 ± 0.059	-0.002	-0.033 ± 0.065	-0.035 ± 0.062	-0.002
				Fe II	11	0.010 ± 0.026	0.009 ± 0.037	-0.001	0.010 ± 0.026	0.009 ± 0.037	-0.001
Tr 12	5790	4.49	2.08	Fe I	29	-0.051 ± 0.058	-0.052 ± 0.058	-0.001	-0.048 ± 0.055	-0.049 ± 0.056	-0.001
				Fe II	16	0.000 ± 0.060	0.001 ± 0.067	0.001	-0.001 ± 0.061	0.000 ± 0.066	0.001
Tr A13	5360	4.53	2.14	Fe I	27	-0.003 ± 0.047	-0.001 ± 0.045	0.002	-0.017 ± 0.051	-0.015 ± 0.049	0.002
				Fe II	10	0.011 ± 0.055	0.019 ± 0.055	0.008	0.011 ± 0.055	0.019 ± 0.055	0.008
Tr 39	4930	2.76	1.96	Fe I	31	-0.063 ± 0.047	-0.082 ± 0.047	-0.019	-0.074 ± 0.050	-0.094 ± 0.050	-0.020
				Fe II	13	-0.020 ± 0.079	-0.039 ± 0.081	-0.019	-0.030 ± 0.074	-0.048 ± 0.076	-0.018

Notes. $^{(a)}$New α value derived from M15. $^{(b)}$Number of lines used to calculate the abundances. $^{(c)}$Abundance derived from new α value model minus abundance derived from old (fixed) α value.

recalibrated α and two other stellar parameters ($T_{\rm eff}$ and log g) more conveniently and accurately.

Even though all the stars in this open cluster have solar-like abundance, there are still different Δ[Fe/H] for different types of stars. We plot the different evolutionary stages of the member stars of our cluster sample in Fig. 2. The Δ[Fe/H] values from Fe I and Fe II lines in the LTE and NLTE cases are also plotted in the Fig. 7 panels. For Tr 183, which is located at the turn-off point, the metallicity discrepancies are above 0.02 dex. The metallicity discrepancies of Tr 183 are relatively large compared to the other cool dwarf stars. As a giant star, Tr 39 also shows a little higher metallicity discrepancy (≈0.02 dex) compared to the

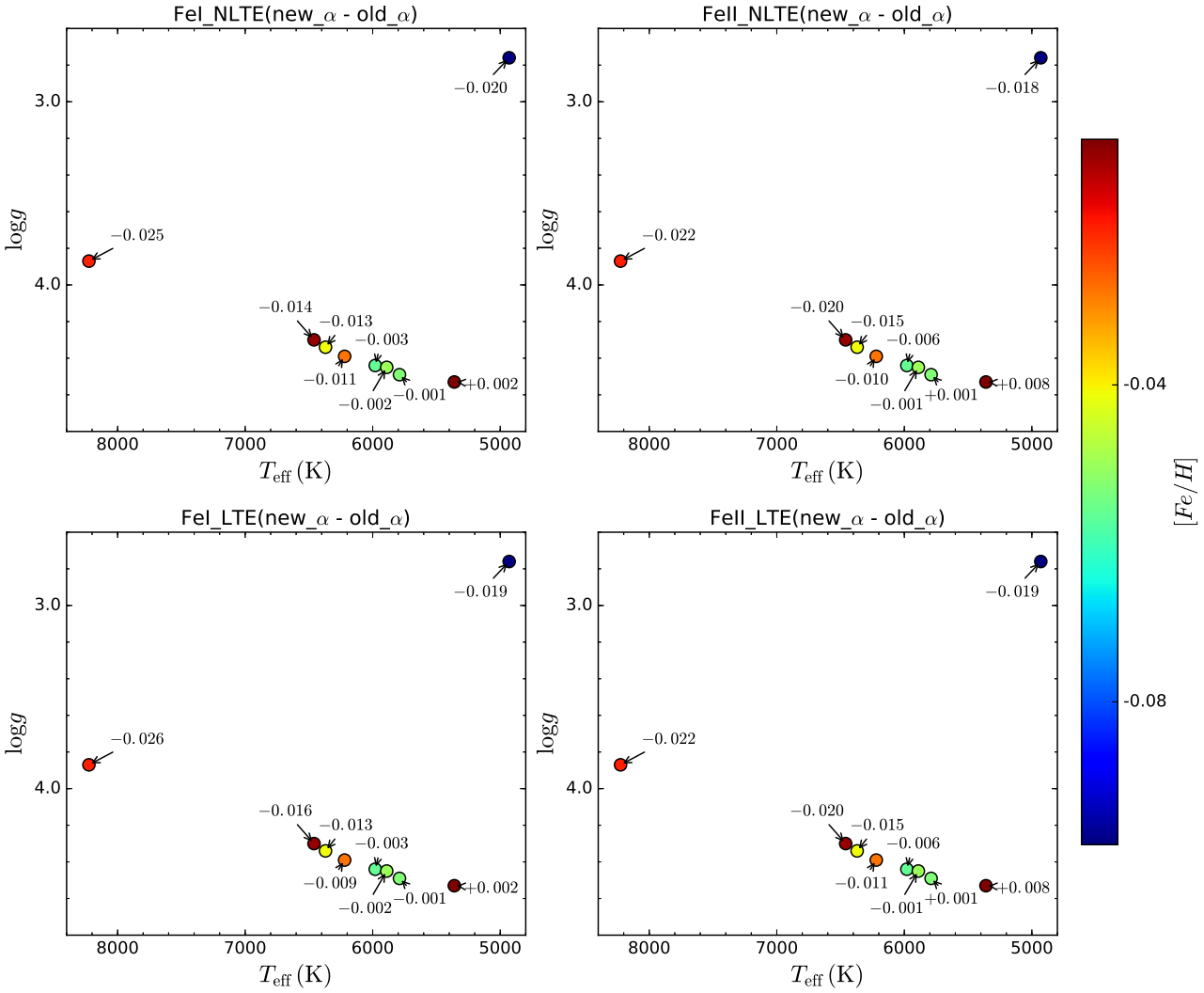

Fig. 7. Discrepancy in [Fe/H] between old and revised α value for the open cluster sample on the HR diagram.

dwarf stars. The higher metallicity discrepancy as caused by evolutionary status is explained by Viani et al. (2018), who showed that differences exist between sets of isochrones with different α values, especially at the turn-off and giant branch.

With regard to the other seven cool dwarf stars, we notice that the stars can be divided into two groups. For the three dwarf stars (Tr 118, Tr 114 and Tr 53) with $T_{\rm eff} \geq 6200$ K, the $|\Delta$[Fe/H]$|$ values are almost higher than 0.01 dex. While for the other four dwarf stars (Tr 65, Tr 85, Tr 12 and Tr A13) with $T_{\rm eff} \leq 5890$ K, the $|\Delta$[Fe/H]$|$ are almost below 0.005 dex. Our results are in agreement with Viani et al. (2018).

Viani et al. (2018) perform a trilinear fit to model $\alpha/\alpha_\odot$ as a function of other stellar atmosphere parameters,

$$\alpha/\alpha_\odot = a + b\log g + c\log(T_{\rm eff}) + d([{\rm Fe/H}]). \quad (2)$$

They fit the equation for different temperature ranges to constrain the corresponding coefficients, a, b, c and d. When $3.73 < \log(T_{\rm eff}) < 3.78$ and $\log(T_{\rm eff}) > 3.78$, the coefficient d is 0.605 and 0.328, respectively. The temperature boundary in our result is very close to that of Viani et al. (2018). In our analysis, we keep $T_{\rm eff}$ and $\log g$ at the same value for our two different α models; therefore, the $\log(T_{\rm eff})$ and $\log g$ terms are taken as constants. The recalibrated α values of the seven dwarf stars are almost equal with $\alpha \approx 2$. Based on Eq. (2), we derive that $\frac{\Delta[{\rm Fe/H}]}{\Delta\alpha} \simeq \frac{\partial[{\rm Fe/H}]}{\partial\alpha} = \frac{1}{d}$. Since the coefficient d of $3.73 < \log(T_{\rm eff}) < 3.78$ is higher than that of $\log(T_{\rm eff}) > 3.78$, therefore the Δ[Fe/H] of $3.73 < \log(T_{\rm eff}) < 3.78$ is lower than that of $\log(T_{\rm eff}) > 3.78$.

We plot Δ[Fe/H] along with $T_{\rm eff}$ and $\log g$ in Figs. 8 and 9, respectively. We can easily identify the turn-off star (Tr 183) and the giant star (Tr 39) in all panels of Δ[Fe/H] – $T_{\rm eff}$ and Δ[Fe/H] – $\log g$. Except for these two stars, the other seven stars demonstrate a linear relationship in all panels. As we discussed above, we separated the seven dwarf stars into two groups: one with $T_{\rm eff} < 6100$ K and another with $T_{\rm eff} > 6100$ K. A clear trend appears when we use linear regression to model Δ[Fe/H] versus $T_{\rm eff}$ (Fig. 8). The linear fit coefficients are shown in Table 4. The slopes differ for $T_{\rm eff} < 6100$ K and $T_{\rm eff} > 6100$ K. For stars with $T_{\rm eff} < 6100$ K, there is no difference in the liner fit coefficients between the LTE and NLTE cases for both Fe I and Fe II lines.

In the Δ[Fe/H] – $\log g$ plane, one linear fit is adequate for all seven dwarf stars (Table 5). If there were more giant stars in our sample, the lower $\log g$ stars (giant stars) might be considered separately as Bonaca et al. (2012) and Viani et al. (2018) suggest. The linear trends between Δ[Fe/H] and $\log g$ are presented in Fig. 9. Everywhere, the value of Δ[Fe/H] decreases with decreasing $\log g$ for the dwarf stars. There are only small

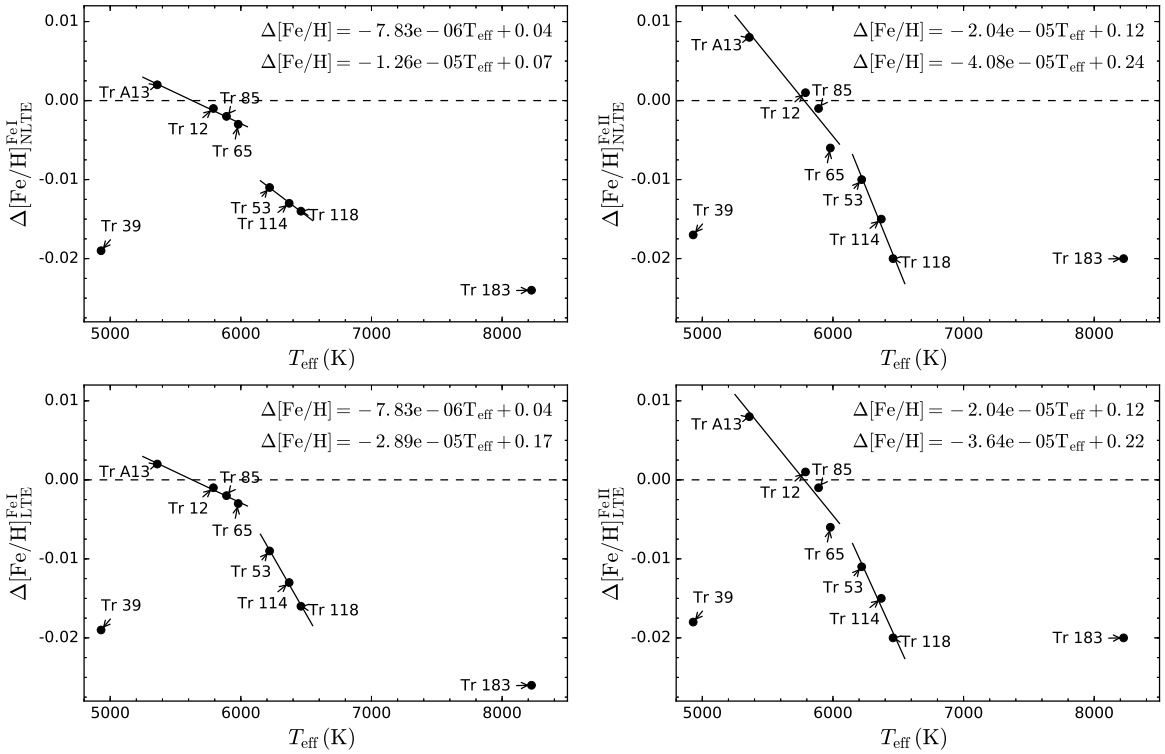

Fig. 8. Discrepancy in [Fe/H] between old and revised α value for the open cluster sample along with $T_{\rm eff}$.

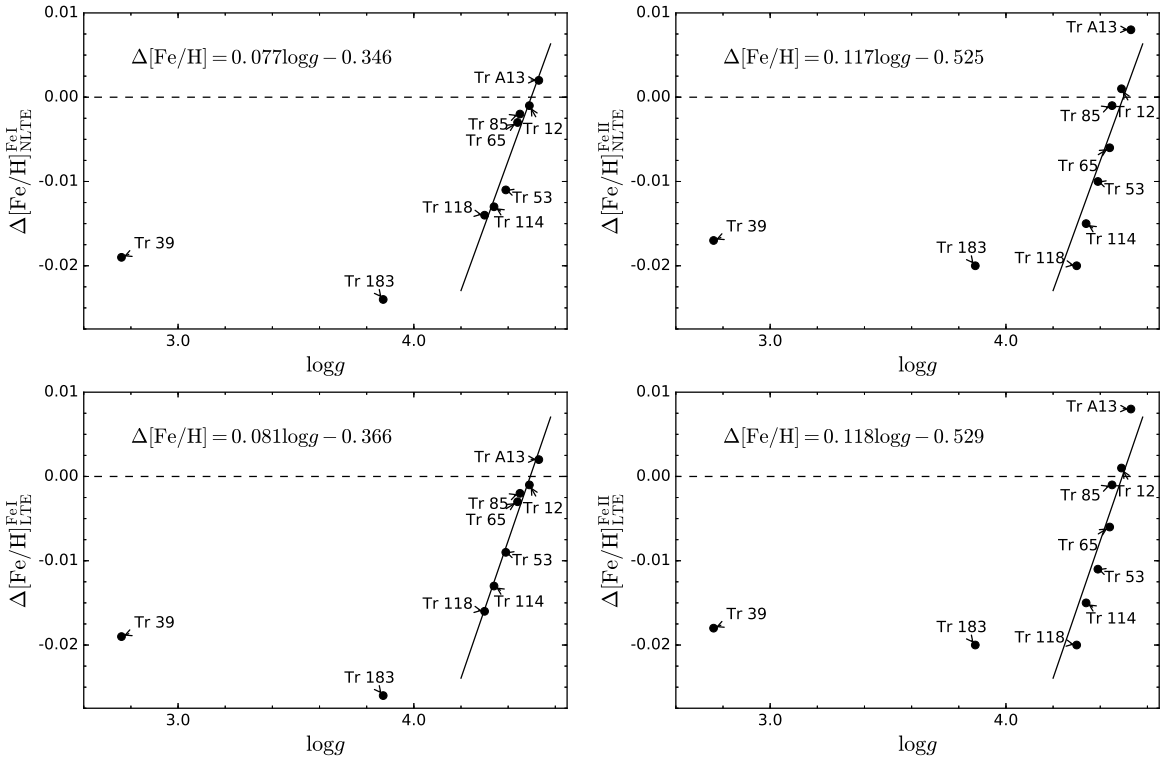

Fig. 9. Discrepancy in [Fe/H] between old and revised α value for the open cluster sample along with log g.

differences between LTE and NLTE cases in the coefficients for both Fe I and Fe II lines.

5. Conclusions

In this work we studied how the mixing-length parameter α influences the determination of metallicity in FGK type stars. We analyzed the metallicities of stars from a field star sample and open cluster with two α values, fixed solar-calibrated α, and α obtained for each star individually. The metallicity discrepancy was defined as Δ[Fe/H] = [Fe/H]$_{\alpha_{\rm new}}$ − [Fe/H]$_{\alpha_{\odot=0.82}}$. Both samples were analyzed in a homogeneous manner. The accurate iron abundance measurements were done line by line based on high resolution and high signal-to-noise ratio (S/N) observed

Table 4. Linear fit coefficients of Δ[Fe/H] − $T_{\rm eff}$.

Δ[Fe/H] = $aT_{\rm eff} + b$				
	LTE		NLTE	
	a	b	a	b
Fe I $T_{\rm eff} < 6100K$	− 7.83e-6	0.04	− 7.83e-6	0.04
Fe I $T_{\rm eff} > 6100K$	− 2.89e-5	0.17	− 1.26e-5	0.07
Fe II $T_{\rm eff} < 6100K$	− 2.04e-5	0.12	− 2.04e-5	0.12
Fe II $T_{\rm eff} > 6100K$	− 3.64e-5	0.22	− 4.08e-5	0.24

Table 5. Linear fit coefficients of Δ[Fe/H] − log g.

Δ[Fe/H] = $a \log g + b$				
	LTE		NLTE	
	a	b	a	b
Fe I	0.081	− 0.366	0.077	− 0.346
Fe II	0.118	− 0.529	0.117	− 0.525

spectra for both Fe I and Fe II lines. The NLTE effects for the iron lines of two ionization stages were also considered during the analysis, although there are no visible differences in metallicity discrepancies Δ[Fe/H] owing to revised α between the LTE and NLTE cases. We next summarize our conclusions after our aforementioned analysis of each star.

For the FGK dwarf field stars, we find a minor impact of α on the metallicity determination, where the |Δ[Fe/H]| caused by the α correction is less than 0.02 dex, while for one turn-off star and the giant stars the |Δ[Fe/H]| can reach up to ~0.03 dex. For the metal-poor giants in the field star sample, the |Δ[Fe/H]| is slightly higher by about ~0.003 compared to the |Δ[Fe/H]| of solar metallicity giant star from the open cluster sample even though they have relatively lower $\Delta\alpha$ values. The derived |Δ[Fe/H]| does not exceed 0.03 dex, that is lower than typical uncertainties in metallicity, which is about 0.05–0.06 dex (Ryabchikova et al. 2016) for main-sequence stars. The fixed solar mixing-length values adopted in the stellar atmosphere models should be considered cautiously, especially for turn-off and giant stars. Otherwise, it should be taken into account in the total error estimation of metallicity.

For the open cluster sample, we investigated the correlation between Δ[Fe/H] caused by revised α with stellar parameters. We derived linear Δ[Fe/H] versus $T_{\rm eff}$ and Δ[Fe/H] versus log g relations for main-sequence stars. For the giant stars, we need to analyze more stars to investigate the Δ[Fe/H] versus $T_{\rm eff}$ and Δ[Fe/H] versus log g relations in the future. Our obtained relations are useful for roughly estimating Δ[Fe/H] for solar metallicity FGK dwarf stars.

In summary, the metallicity discrepancy caused by α corrections are less than the typical metallicity uncertainties in most cases. If accurate metallicity measurements are secured, the proper mixing-length α in the model calculations should be considered. In this paper, we focused on Fe I and Fe II to understand the impact of convection on metallicity. An investigation into how the convection mixing-length parameter influences other atomic and molecular lines will be done in further work. The elements we seek to analyze are, for example, the strong lines of magnesium and calcium as well as the CH and C2 bands, especially in metal-poor star samples. A comparison of the MLT impact on the metallicity determination between the Böhm-Vitense (1958) and Canuto & Mazzitelli (1991, 1992) formulations will be considered in a future paper.

Acknowledgements. This work was supported by the National Natural Science Foundation of China under grant Nos. 11988101, 11890694, 11773033 and the National Key R&D Program of China No. 2019YFA0405502. We thank the anonymous referee for the valuable suggestions and comments. We thank L. Mashonkina for providing NLTE calculations, J.R. Shi for many helpful discussion. N.S. thanks K.F. Tan and J.B. Zhang for their guidance in performing the line formation analysis.

References

Asplund, M. 2005, ARA&A, 43, 481
Bernkopf, J. 1998, A&A, 332, 127
Böhm-Vitense, E. 1958, Z. Astrophys., 46, 108
Bonaca, A., Tanner, J. D., Basu, S., et al. 2012, ApJ, 755, L12
Bounatiro, L. 1993, A&AS, 100, 531
Butler, K., & Giddings, J. 1985, Newsletter on the analysis of astronomical spectra, No. 9, University of London
Canuto, V. M., & Mazzitelli, I. 1991, ApJ, 370, 295
Canuto, V. M., & Mazzitelli, I. 1992, ApJ, 389, 724
Casewell, S. L., Jameson, R. F., & Dobbie, P. D. 2006, MNRAS, 365, 447
Castelli, F., & Kurucz, R. L. 2004, ArXiv e-prints [arXiv: astro-ph/0405087]
Chun, S.-H., Yoon, S.-C., Jung, M.-K., Kim, D. U., & Kim, J. 2018, ApJ, 853, 79
Fuhrmann, K., Axer, M., & Gehren, T. 1993, A&A, 271, 451
Fuhrmann, K., Pfeiffer, M., Frank, C., Reetz, J., & Gehren, T. 1997, A&A, 323, 909
Gaia Collaboration (Babusiaux, C., et al.) 2018, A&A, 616, A10
Grupp, F. 2004a, PhD thesis, Ludwig-Maximilians-Universität München, München, Germany
Grupp, F. 2004b, A&A, 420, 289
Grupp, F. 2004c, A&A, 426, 309
Guenther, D. B., & Demarque, P. 2000, ApJ, 531, 503
Gustafsson, B., Edvardsson, B., Eriksson, K., et al. 2008, A&A, 486, 951
Joyce, M., & Chaboyer, B. 2018a, ApJ, 864, 99
Joyce, M., & Chaboyer, B. 2018b, ApJ, 856, 10
Kupka, F., Piskunov, N., Ryabchikova, T. A., Stempels, H. C., & Weiss, W. W. 1999, A&AS, 138, 119
Kurucz, R. L. 1993, SYNTHE Spectrum Synthesis Programs and Line Data (Cambridge, MA: Smithsonian Astrophysical Observatory)
Kurucz, R. L., Furenlid, I., Brault, J., & Testerman, L. 1984, Solar flux atlas from 296 to 1300 nm (New Mexico: National Solar Observatory)
Lodders, K., Palme, H., & Gail, H.-P. 2009, Landolt Börnstein (Berlin: Springer)
Ludwig, H. G., Freytag, B., & Steffen, M. 1999, A&A, 346, 111
Magic, Z., Weiss, A., & Asplund, M. 2015, A&A, 573, A89
Marigo, P., Girardi, L., Bressan, A., et al. 2017, ApJ, 835, 77
Mashonkina, L., Gehren, T., Shi, J.-R., Korn, A. J., & Grupp, F. 2011, A&A, 528, A87
Mashonkina, L., Sitnova, T., Yakovleva, S. A., & Belyaev, A. K. 2019, A&A, 631, A43
Mermilliod, J.-C., Grenon, M., & Mayor, M. 2008, A&A, 491, 951
Miglio, A., & Montalbán, J. 2005, A&A, 441, 615
Nissen, P. E., Hoeg, E., & Schuster, W. J. 1997, ESA SP, 402, 225
Pfeiffer, M. J., Frank, C., Baümller, D., Fuhrmann, K., & Gehren, T. 1998, A&AS, 130, 381
Reetz, J. K. 1999, PhD thesis, Ludwig-Maximilians-Universität München, München, Germany
Ryabchikova, T., Piskunov, N., Pakhomov, Y., et al. 2016, MNRAS, 456, 1221
Rybicki, G. B., & Hummer, D. G. 1991, A&A, 245, 171
Rybicki, G. B., & Hummer, D. G. 1992, A&A, 262, 209
Silaj, J., & Landstreet, J. D. 2014, A&A, 132, A1
Trampedach, R., Stein, R. F., Christensen-Dalsgaard, J., Nordlund, k., & Asplund, M. 2014, MNRAS, 445, 4366
Trumpler, R. J. 1938, Lick Observ. Bull., 18, 167
Valle, G., Dell'Omodarme, M., Prada Moroni, P. G., & Degl'Innocenti, S. 2019, A&A, 623, A59
Viani, L. S., Basu, S., Joel Ong J. M., Bonaca, A., & Chaplin, W. J. 2018, ApJ, 858, 28
Wu, X. S., Alexeeva, S., Mashonkina, L., et al. 2015, A&A, 577, A134
Yakovleva, S. A., Belyaev, A. K., & Kraemer, W. P. 2018, Chem. Phys., 515, 369
Yakovleva, S. A., Belyaev, A. K., & Kraemer, W. P. 2019, MNRAS, 483, 5105